Check for updates

TECHNICAL ARTICLE

In-Situ X-Ray Imaging High Strain Rate Compression of Laminate Al-Graphene Composite and Mechanical Property Characterization

GUANG YANG, 1 DONGXUE XIE, 2 YIZHOU NIE, 3 XUEDONG ZHAI, 3 NESREDIN KEDIR, 4 WEINONG CHEN, 3,4 A.P.S. GAUR, 1 SUPREM R. DAS, 1,5 SHUTING LEI, 1 KAMEL FEZZAA, 6 JIAN WANG, 2,8 and DONG LIN 1,7,9

1.—Industrial and Manufacturing Systems Engineering, Kansas University, Manhattan, KS 66506, USA. 2.—Department of Mechanical and Materials Engineering, University of Nebraska Lincoln, Lincoln, NE 68588, USA. 3.—School of Purdue West Aeronautics and Astronautics, University, 701 Stadium West Lafayette, IN 47907, USA. 4.—School of Materials Engineering, University, West Lafayette, IN 47907, USA. 5.-Mike Wiegers Department of Electrical and Computer Engineering, Kansas State University, Manhattan, KS 66506, USA. 6.—X-Ray Science Division, Argonne National Laboratory, 9700 S. Cass Ave, Lemont, IL 60439, USA. 7.—School of Mechanical, Industrial. and Manufacturing Engineering, Oregon State University, 218 Dearborn Hall, Corvallis, OR 97331, USA. 8.—e-mail: jianwang@unl.edu. 9.—e-mail: dong.lin@oregonstate.edu

Owing to the opaque nature of the laminated structures, traditional high-speed optical camera cannot be used to detect the dynamic process of subsurface deformation. In this article, we report a study of using high speed X-ray imaging to study the high strain rate deformation in laminated Al structures. We used a Kolsky bar apparatus to apply dynamic compression and a high-speed synchrotron X-ray phase contrast imaging (PCI) setup to conduct the in situ X-ray imaging study. The in situ X-ray imaging captures the shock wave propagation in the laminated structures. After shock compression, we characterized the microstructures by using transmission electron microscopy (TEM), which demonstrates an increase of dislocation density. The micropillar compression tests show that the yield strength at 0.2% offset of laminated Al-graphene composite has a significant increase of 67%, from 30 to 50 MPa, compared to laminate Al after shock loading.

INTRODUCTION

Next-generation structural, energy, and defense materials need to withstand mechanical extremes, such as shock compression, without failure. Shock compression occurs in a wide variety of situations, including high-speed automobile and aircraft collisions, explosive welding, armor penetration, meteor impacts, interstellar dust-dust collisions, and inertial confinement fusion. All of these situations rely on

Guang Yang and Dongxue Xie have equally contributed to this work.

material performance as critical to safety and survival. Different experimental techniques, such as quasi-static measurements, shock compression, and quasi-isentropic compression, have been applied to study the aforementioned experimental conditions. Recently, experimental techniques enabling shock compression using Kolsky bar have generated growing interest. ^{3–17}

The state-of-the-art techniques utilize high density of interfaces in nanolaminate metals to withstand shock compression. A paradox to enhancing the penetration resistance under shock loading is that the interfaces should be weak and strong simultaneously. On one hand, a weak interface can weaken shock waves because of their high shock wave

Published online: 22 May 2023

resistance, while the interfaces may be destroyed when a shock wave passes them. On the other, strong interfaces can constrain the propagation of dislocations and heal the materials, while shock waves with high frequencies can coherently pass them. These shock-induced microstructural changes in metals have been correlated with variations in the post-shock mechanical properties, leading to increases in both the hardness and reload yield strength. ²⁰

In this report, the Kolsky bar was used to apply shock compression in laminated Al-graphene composites, which were assembled by transferring single layer graphene between Al sheets. Graphene is a planar monolayer of carbon arranged as a two-dimensional (2D) lattice with ultra-large specific surface area ratio (2600 m²/g) and the highest known Young's modulus with only a single atomic layer of carbon atoms arranged in two dimensions with a sp^2 bonding configuration.^{21,22} High-speed X-ray imaging was applied to observe the shock wave propagation inside the laminated Al structures. After shock compression, the microstructure in Al sheets was studied by highresolution transmission electron microscopy (TEM), which showed high density of dislocations generated in the cross section. The mechanical properties were characterized by micro-pillar compression.

MATERIALS AND METHODS

Laminated Al-Graphene Composite Sample Preparation

The aluminum/graphene laminate composites were fabricated by inserting an alternate graphene layer as a reinforcement layer to the aluminum foils and with subsequent application of a pressure perpendicular to the plane of the layers. High-purity aluminum foil [thickness 25 μm (Alfa Aesar, product number 10558, 99.45% metal basis)] was used as the metal matrix, and a chemical vapor deposited single layer graphene (originally on copper foil, Graphene supermarket) was used as the atomic membrane between aluminum foil. Both the aluminum foil and the copper/graphene were punched into circular shapes. Copper was etched using a copper etchant as used in the standard graphene transfer process. Then, the graphene was carefully transferred onto the aluminum disc in such a way that it was perfectly aligned onto its surface without any visible wrinkles and folds. A total of nine such aluminum discs were coated each with a transferred graphene layer. Then, the whole stack with another top aluminum foil was filled into a ring-shaped mold and was hot pressed at 300 °C with a pressure of \sim 20 MPa. After releasing the pressure, the laminated aluminum-graphene composites were used as experimental samples.

In Situ X-ray Imaging Setup

The high-speed X-ray imaging experiments were conducted at the beam line 32-ID-B, Advanced Photon Source (APS), Argonne National Laboratory.

The setup of the in situ X-ray imaging is schematically shown in Fig. 1. The fundamental energy of the X-rays was centered at 25.0 keV. The size of the X-ray beam on the sample was 2.56 mm * 1.5 mm with an intensity of 1.4 * 1016 photons/s/mm²/0.1% BW. The process dynamics was recorded at 5 MHz frame rate with a Shimadzu HPV-X2 high-speed camera. Appropriate time delays need to be calibrated prior to the experiments to synchronize the camera with the start of the loading and passing of the X-rays through the specimen to capture the event. The resolution of the imaging system was estimated to be 6.4 μ m/pixel, and the frame size was 100,000 pixels (400 * 250 pixels).

Kolsky Compression Bar

A Kolsky bar, with normal high strain rates $(10^2 - 10^5 \text{ s}^{-1})$, was used to apply the dynamic loading. The Kolsky bar used in this report is composed of a striker bar (diameter = 12.7 mm, length = 76 mm) and incident bar (diameter = 12.7 mm, length = 1372 mm), both manufactured from a high-strength steel alloy (Vascomax 300 maraging steel).

Microstructure Characterization

TEM specimens of cross sections were prepared by FIB lifting-out. The preparations were performed by using FEI Helios 660 dual-beam system. The thin foils were cut by using Ga + with a voltage of 30 kV and currents from 15 nA to 50 pA. To remove a possible damage layer, the surfaces of specimens were polished by using Ga⁺ with a voltage of 5 kV and currents of 3.2 nA. The structural characterization was conducted using FEI Tecnai Osiris transmission electron microscope operated at 200 kV.

Mechanical Properties Characterization

The micro-pillars were prepared on the sample before and after shock loading. FEI Helios 660 dual-beam system was used in the preparation process. The micro-pillars have a diameter of 5 μ m and height of 10 μ m. In situ compression tests were conducted on the pillars by using Hysitron PI85 PicoIndenter in FEI Helios 660 dual-beam system. The strain rate was set to 10^{-3} s⁻¹.

RESULTS

The behaviors of the Al-graphene composites under shock compression were studied in repeated experimental conditions. The high-speed image sequences of a representative experiment are shown in Fig. 2. The dashed curves indicate the location of the plastic shock wave front at a specific time. The shock loading was initiated from the left side of the sample by the Kolsky compression bar, and the plastic shock wave propagated along the shock direction until it hit the right boundary of the sample. The in situ X-ray study captured the shock

In-Situ X-Ray Imaging High Strain Rate Compression of Laminate Al-Graphene Composite and Mechanical Property Characterization

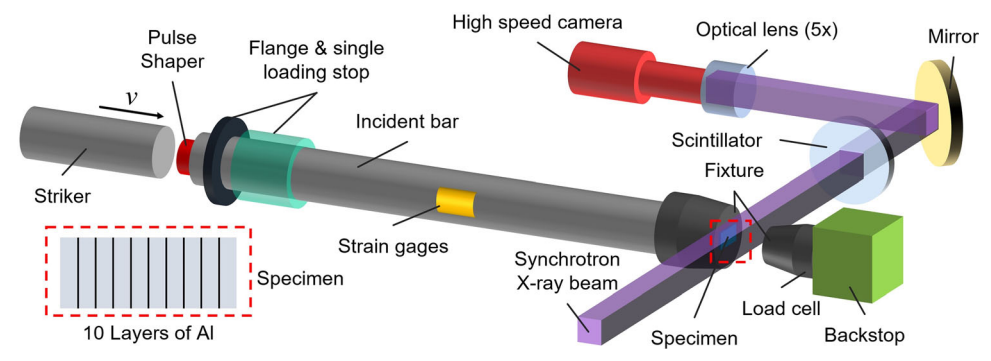


Fig. 1. In situ gas gun compression setup. Specimen contains ten layers of aluminum foils. One single layer of graphene was transferred on the surface of each aluminum foil.

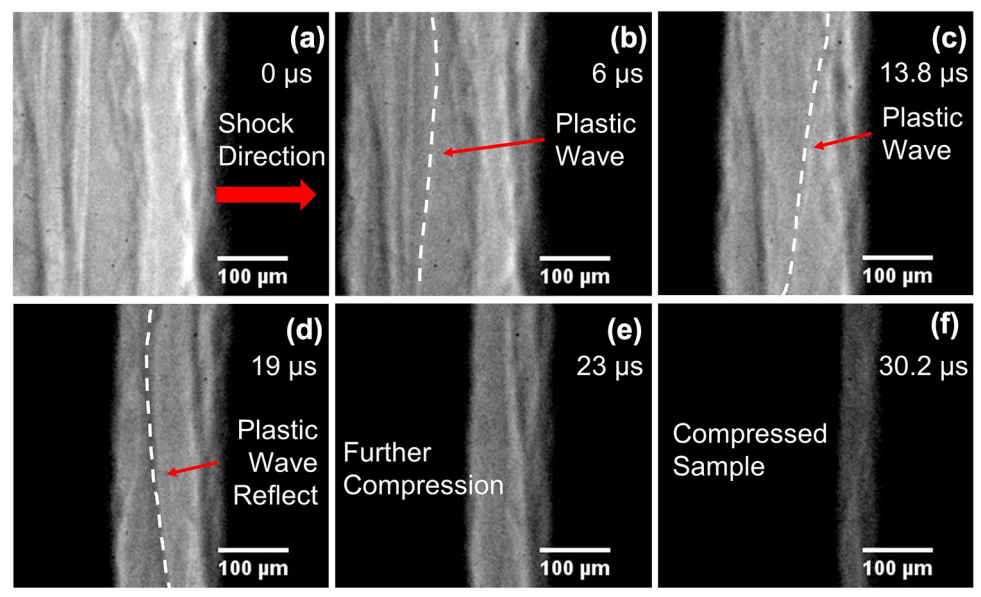


Fig. 2. High speed in situ X-ray imaging of Al-graphene composites under shock compression test. (a) Initial status, (b-d) shock wave propagation, (e) further compression, and (f) final compressed sample.

wave propagation in the cross section of laminated Al-graphene composite (Fig. 2a). The plastic wave propagation (Fig. 2b-c), reflection (Fig. 2d), and final compressed sample (Fig. 2e) are clearly observed by in situ X-ray imaging. Figure 2d shows that the wave was reflected for a short distance before the sample was fully compressed. The average speed of the plastic wave was calculated as around 38.85 m/s.

After shock loading, the microstructure of the Al was characterized by using TEM. The bright-field image of the sample without shocking is shown in Fig. 3 a. The specimen was extracted from the surface of the sample. This specimen contained the material from surface to the area with a depth of $10~\mu m$. There was no grain boundary within the specimen. The diffraction pattern, as shown in Fig. 3b, was taken from < 110 > axis. This pattern

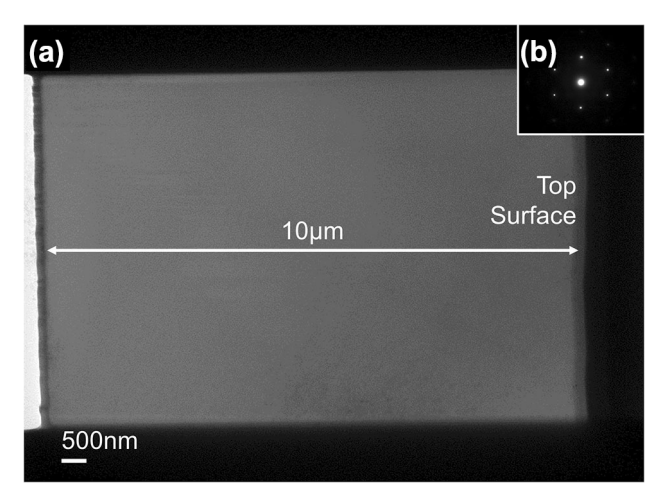


Fig. 3. (a) TEM bright-field image of sample before shocking experiment. (b) Selected area electron diffraction pattern of the specimen in (a).

was consistent with a standard pattern of an FCC structure, which indicates that this specimen was a single crystal.

The microstructure of the gas gun-shocked Algraphene composite was also characterized. Figure 4a shows a bright-field image of the shocked sample. Many grain boundaries were observed in this specimen. A grain boundary was magnified, and HRTEM images are shown in Fig. 4b and 4c. Their FFT pattern is shown in Fig. 4d. From this pattern, two sets of < 110 > patterns were observed with small orientation differences.

Comparing the TEM image of the sample before and after shocking, there is little contrast in the sample before shocking, and there are strips in the shocked sample. The uniform image of the sample without shocking indicates the low dislocation density and large grains. The strips in the shocked sample are small elongated grains. The dark region in these grains suggests that there are more dislocations. The misorientation between grains was relatively small. Considering the fact that these grains were formed during shocking, these low-angle grain boundaries might be produced by the accumulation of dislocations.

The micro-pillars were prepared on the sample before and after shock loading. The image of micropillar after preparation is shown in Fig. 5a, c for unshocked and shocked samples, respectively. The micro-pillars have a diameter of 5 μ m and height of 10 μ m. The in situ compression tests were performed on these micro-pillars. Figure 5b, d shows the micro-pillars after compression tests. For unshocked micro-pillar, slip mainly occured on one plane. The activation of slip systems was controlled by Schmid's factor since the Al micro-pillar is a single crystal. It is reasonable that only one slip system has a large Schmid's factor and was activated. For the polycrystalline shocked pillar, multiple slip traces appeared on the surface of the shocked pillar because different grains have different favored slip systems.

The engineering stress-strain curves of compression tests are presented in Fig. 6. The curves showed that the yield strengths at 0.2% were 30 MPa and 50 MPa for unshocked and shocked samples, respectively. The yield strength of the shocked sample was 67% higher than that of the untreated sample. The untreated micro-pillar was compressed to a strain of 6.8% with a stress of 52 MPa. The stress in the shocked micro-pillar at the same strain level was 72 MPa. The maximum strain of the shocked pillar was 14.3% with a stress of 84 MPa. More load drops occurred during the compression test of the unshocked sample.

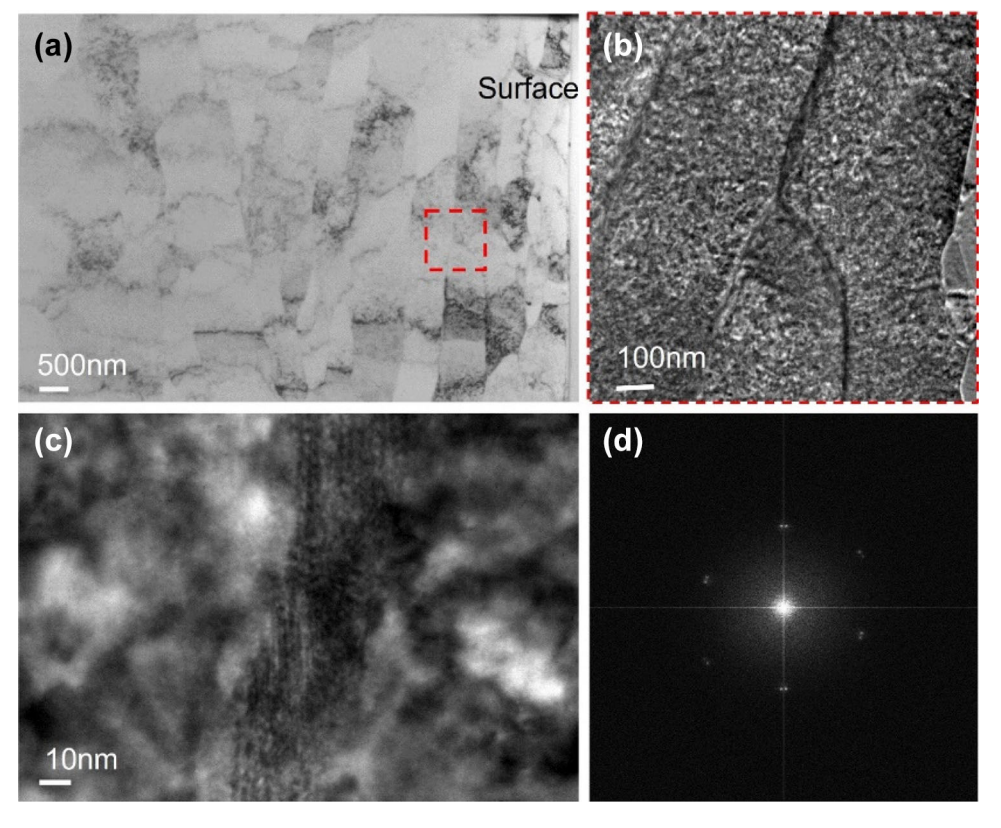


Fig. 4. (a) TEM bright-field image of sample after shocking experiment. (b) Magnified bright-field image of the area in red box, showing grain boundaries. (c) HRTEM image of a segment of grain boundary in (b). (d) FFT patten of the HRTEM image in (c) (Color figure online).

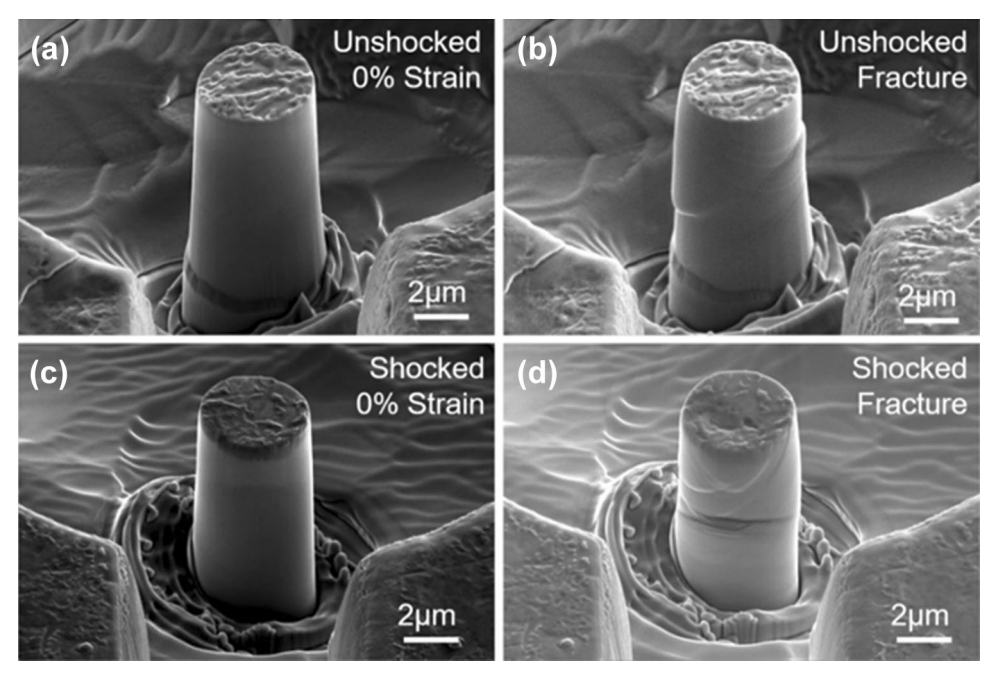


Fig. 5. (a) and (b) SEM images of micro-pillar before and after compression test on the unshocked sample. (c) and (d) SEM images of micro-pillar before and after compression test on the shocked sample.

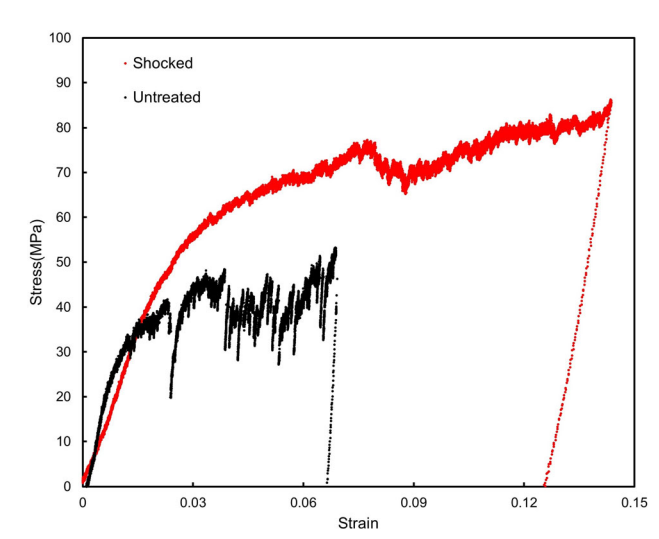


Fig. 6. Stress-strain curve from micro-pillar compression tests.

CONCLUSION

The response of laminated Al-graphene composite under gas gun shock loading was revealed by high-speed dynamic X-ray imaging. The shock wave propagation in the laminated structures was observed, and the shock wave speed was calculated from these images. The microstructure, such as dislocation, after shock loading showed a high dislocation owing to the high strain rate deformation. The mechanical properties, which were characterized by micro-pillar compression, of Al-graphene composites are significantly improved after shock loading. The ultimate stress and strain

for untreated Al-graphene composite were measured as 52 MPa and 6.8%, while the ultimate stress and strain for shocked Al-graphene composite were 84 MPa and 14.3%. This work demonstrates an effective strategy to enhance the mechanical properties of metal-graphene composites, leading to broader applications as structural, energy, and defense materials.

ACKNOWLEDGEMENTS

This research used resources of the Advanced Photon Source, a US Department of Energy (DOE) Office of Science User Facility operated for the DOE Office of Science by Argonne National Laboratory under Contract No. DE-AC02-06CH11357. D. L. appreciates the support from the National Science Foundation under Award No. 1943445. The in situ micromechanical tests were performed in the Nebraska Center for Materials and Nanoscience, which is supported by the National Science Foundation under Award ECCS: 1542182 and the Nebraska Research Initiative.

CONFLICT OF INTEREST

The authors declare that they have no conflict of interest.

REFERENCES

- N.A. Mara, C.A. Bronkhorst and I.J. Beyerlein, Los Alamos National Lab.(LANL), Los Alamos, NM (United States) 2015
- E. Bringa, K. Rosolankova, R. Rudd, B. Remington, J. Wark, M. Duchaineau, D. Kalantar, J. Hawreliak, and J. Belak, Nat. Mater. 5, 805–809 (2006).

- W.W. Chen, M.C. Hudspeth, B. Claus, N.D. Parab, J.T. Black, K. Fezzaa, and S.N. Luo, *Philos. Trans. R. Soc. A Math. Phys. Eng. Sci.* 372, 20130191 https://doi.org/10.1098/rsta.2013.0191 (2014).
- N.D. Parab, J.T. Black, B. Claus, M. Hudspeth, J. Sun, K. Fezzaa, and W.W. Chen, *Int. J. Appl. Glass Sci.* 5, 363–373 h ttps://doi.org/10.1111/ijag.12092 (2014).
- M.B. Zbib, N.D. Parab, W.W. Chen, and D.F. Bahr, Powder Technol. 283, 57–65 https://doi.org/10.1016/j.powtec.2015.0 4.066 (2015).
- N.D. Parab, Z.A. Roberts, M.H. Harr, J.O. Mares, A.D. Casey, I.E. Gunduz, M. Hudspeth, B. Claus, T. Sun, K. Fezzaa, S.F. Son, and W.W. Chen, Appl. Phys. Lett. 109, 131903 https://doi.org/10.1063/1.4963137 (2016).
- N.D. Parab, Z. Guo, M. Hudspeth, B. Claus, B.H. Lim, T. Sun, X. Xiao, K. Fezzaa, and W.W. Chen, *Philos. Trans. R. Soc. A Math. Phys. Eng. Sci.* 375, 20160178 https://doi.org/10.1098/rsta.2016.0178 (2017).
- Z. Guo, M.J. Forrestal, S. Martinez-Morales, and W. Chen, J. Dyn. Behav. Mater. 5, 409–415 https://doi.org/10.1007/s4 0870-019-00200-3 (2019).
- N. Kedir, C.D. Kirk, Z. Guo, N.E. Kerschen, T. Sun, K. Fezzaa, and W. Chen, *Int. J. Impact Eng.* 129, 168–179 h ttps://doi.org/10.1016/j.ijimpeng.2019.01.012 (2019).
- N.E. Kerschen, C.J. Sorensen, Z. Guo, J.O. Mares, K. Fezzaa, T. Sun, S.F. Son, and W.W. Chen, *Propellants Explos. Pyrotech.* 44, 447–454 https://doi.org/10.1002/prep.201800002 (2019).
- J.O. Mares, Z.A. Roberts, I. EmreGunduz, N.D. Parab, T. Sun, K. Fezzaa, W.W. Chen, S.F. Son, and J.F. Rhoads, *Appl Mater Today* 15, 286–294 https://doi.org/10.1016/j.apmt.2019.01.009 (2019).
- N.D. Parab, L. Xiong, Q. Guo, Z. Guo, C. Kirk, Y. Nie, X. Xiao, K. Fezzaa, W. Everheart, W.W. Chen, L. Chen, and T. Sun, Addit. Manufact. 30, 100878 https://doi.org/10.1016/j.addma.2019.100878 (2019).
- X. Zhai, J. Gao, H. Liao, C.D. Kirk, Y.A. Balogun, and W.W. Chen, *Int. J. Impact Eng.* 129, 112–118 https://doi.org/10.1016/j.ijimpeng.2019.03.002 (2019).

- X. Zhai, J. Gao, Y. Nie, Z. Guo, N. Kedir, B. Claus, T. Sun, K. Fezzaa, X. Xiao, and W.W. Chen, *J. Mech. Phys. Solids* 131, 358–371 https://doi.org/10.1016/j.jmps.2019.07.010 (2019).
- X. Zhai, Z. Guo, J. Gao, N. Kedir, Y. Nie, B. Claus, T. Sun, X. Xiao, K. Fezzaa, and W.W. Chen, *Acta Biomater*. 90, 278–286 https://doi.org/10.1016/j.actbio.2019.03.045 (2019).
- N. Kedir, E. Garcia, C. Kirk, Z. Guo, J. Gao, X. Zhai, T. Sun, K. Fezzaa, S. Sampath, and W.W. Chen, *J Am Ceramic Soc* 103, 4586–4601 https://doi.org/10.1111/jace.17165 (2020).
- X. Zhai, E.A. Nauman, D. Moryl, R. Lycke, and W.W. Chen, J. Mech. Behavior Biomed. Mater. 103, 103597 https://doi. org/10.1016/j.jmbbm.2019.103597 (2020).
- J. Wang, and A. Misra, Curr. Opin. Solid State Mater. Sci. 15, 20–28 https://doi.org/10.1016/j.cossms.2010.09.002 (2011).
- X. Liu, F. Wang, H. Wu, and W. Wang, Appl. Phys. Lett. 104, 231901 (2014).
- G.T. Gray, and J.C. Huang, Mater. Sci. Eng. A 145, 21–35 h ttps://doi.org/10.1016/0921-5093(91)90292-U (1991).
- M. Yang, Y. Liu, T. Fan, and D. Zhang, Prog. Mater. Sci. 110, 100652 https://doi.org/10.1016/j.pmatsci.2020.100652 (2020).
- 22. S. Gadipelli, and Z.X. Guo, *Prog. Mater. Sci.* 69, 1–60 https://doi.org/10.1016/j.pmatsci.2014.10.004 (2015).

Publisher's Note Springer Nature remains neutral with regard to jurisdictional claims in published maps and institutional affiliations.

Springer Nature or its licensor (e.g. a society or other partner) holds exclusive rights to this article under a publishing agreement with the author(s) or other rightsholder(s); author self-archiving of the accepted manuscript version of this article is solely governed by the terms of such publishing agreement and applicable law.